Monoclinic zinc monotungstate Yb^{3+},Li^{+}:$ZnWO_4$: Part II. Polarized spectroscopy and laser operation

Anna Volokitina[a,b], Samuel Paul David[c], Pavel Loiko[d], Kirill Subbotin[e,f], Anatoly Titov[e,f], Denis Lis[e], Rosa Maria Solé[a], Venkatesan Jambunathan[c], Antonio Lucianetti[c], Tomas Mocek[c], Patrice Camy[d], Weidong Chen[g,h], Uwe Griebner[g], Valentin Petrov[g], Magdalena Aguiló[a], Francesc Díaz[a], and Xavier Mateos[a,*]

[a]*Universitat Rovira i Virgili (URV), Física i Cristal·lografia de Materials i Nanomaterials (FiCMA-FiCNA)-EMaS, Marcel.li Domingo 1, 43007 Tarragona, Spain*
[b]*ITMO University, Kronverkskiy Pr., 49, 197101 Saint-Petersburg, Russia*
[c]*HiLASE Centre, Institute of Physics of the Czech Academy of Sciences, Za Radnicí 828, 25241 Dolní Břežany, Czech Republic*
[d]*Centre de Recherche sur les Ions, les Matériaux et la Photonique (CIMAP), UMR 6252 CEA-CNRS-ENSICAEN, Université de Caen Normandie, 6 Boulevard du Maréchal Juin, 14050 Caen Cedex 4, France*
[e]*Prokhorov General Physics Institute, Russian Academy of Sciences,38 Vavilova St., 119991 Moscow, Russia*
[f]*Mendeleev University of Chemical Technology of Russia, 9 Miusskaya Sq., 125047 Moscow, Russia*
[g]*Max Born Institute for Nonlinear Optics and Short Pulse Spectroscopy, Max-Born-Str. 2a, 12489 Berlin, Germany*
[h]*Key Laboratory of Optoelectronic Materials Chemistry and Physics, Fujian Institute of Research on the Structure of Matter, Chinese Academy of Sciences, Fuzhou, 350002 Fujian, China*

**Corresponding author, e-mail: xavier.mateos@urv.cat*

Abstract. Monoclinic ytterbium-lithium codoped zinc monotungstate crystal (Yb^{3+},Li^{+}:$ZnWO_4$) is a promising material for laser opertation at ~1.06 μm. Absorption, σ_{abs}, and stimulated-emission, σ_{SE}, cross-sections are determined for light polarized along the optical indicatrix axes, $\boldsymbol{E} \parallel N_p$, N_m and N_g. At room temperature, the maximum σ_{SE} amounts to 2.81×10^{-20} cm^2 at 1055.6 nm (for $\boldsymbol{E} \parallel N_p$) and the gain bandwidth reaches ~22 nm (for $\boldsymbol{E} \parallel N_g$). The radiative lifetime of the upper laser level is 0.37 ms. The Stark splitting of Yb^{3+} multiplets is resolved with low-temperature (6 K) spectroscopy revealing a relatively large total splitting of the ground-state, $\Delta E(^2F_{7/2}) = 804$ cm^{-1}, being remarkably high as compared to other Yb^{3+}-doped tungstate crystals. A notable inhomogeneous broadening of the zero-phonon line is detected at 6 K. A continuous-wave diode-pumped 1.8 at.% Yb^{3+},Li^{+}:$ZnWO_4$ laser generated a maximum output power of 2.90 W at ~1059 nm with a slope efficiency of 57.9% and a linearly polarized

output ($\boldsymbol{E} \parallel N_p$). Yb^{3+},Li^{+}:$ZnWO_4$ is attractive for broadbly tunable and mode-locked oscillators.

Keywords: zinc tungstate; ytterbium lasers; optical spectroscopy; Stark splitting; luminescence; laser operation.

1. Introduction

The ytterbium (Yb^{3+}) ion (electronic configuration: $[Xe]4f^{13}$) is a major subject of research on laser emission at ~1 μm owing to its $^2F_{5/2} \rightarrow {}^2F_{7/2}$ transition. This is because of the following advantages: (i) easy pumping by commercial InGaAs laser diodes emitting at ~0.96-0.98 μm [1-3], (ii) simple energy-level scheme leading to high laser efficiencies and weak heat loading [4,5], (iii) larger Stark splitting of the ground-state ($^2F_{7/2}$) as compared with Nd^{3+} ion, leading to broader wavelength tunability and the generation of ultrashort pulses in mode-locked (ML) lasers [6], (iv) the absence of parasitic energy-transfer processes [7].

Tungstate crystals with different crystallographic structures are known as excellent hosts for Yb^{3+} doping [8-11]. In general, they benefit from high transition cross-sections for polarized light [8], broad emission bands which are attractive for sub-100 fs ML lasers [6,9] and strong Raman activity making self-frequency Raman conversion feasible [12].

A prominent example is the crystal family of monoclinic (sp. gr. *C*2/*c*) potassium (rare-earth) double tungstates Yb:$KRE(WO_4)_2$ where RE = Gd, Y or Lu [8,13]. These crystals feature a substitutional rare-earth site (symmetry: C_2) and easy Yb^{3+} doping. Efficient continuous-wave (CW) [14,15], passively Q-switched (PQS) [16] and ML [6,17] Yb:$KRE(WO_4)_2$ lasers are known. The drawback of these materials as laser gain media is their moderate thermal conductivity ($\langle\kappa\rangle$ = 3.1 $Wm^{-1}K^{-1}$ for $KLu(WO_4)_2$ [18]) and strong anisotropic thermal expansion [19]. Another difficulty is that all the $KRE(WO_4)_2$ representatives exhibit a polymorphic phase transformation below the melting point and the monoclinic low-temperature phase (α-phase) of interest for lasing cannot be directly obtained from the melt, therefore the Top-Seeded Solution Growth (TSSG) method (using a flux) [8] is needed for the growth of these crystals.

A second family of tungstate crystals deeply studied for Yb^{3+} doping comprises materials with a general chemical formula of $ARE(WO_4)_2$ (where A = Li or Na and RE = La, Gd, Y, Lu or Bi) [9,20-22]. These crystals belong to the tetragonal class (having a scheelite-like structure, sp. gr. $I4_1/a$) and they are structurally disordered, as the A^+ and RE^{3+} cations share two non-equivalent sites (2*b* and 2*d*) [22]. This leads to a significant inhomogeneous broadening of Yb^{3+} emission bands. Laser action in Yb^{3+}-doped $ARE(WO_4)_2$ crystals was demonstrated and they were found particularly attractive for ML oscillators [9]. The majority of scheelite-like double tungstate crystals can be grown by the Czochralski (Cz) method (from the melt) [23]. Because of the disordered structure, the thermal conductivity of these crystals is relatively low, $\langle\kappa\rangle$ ~1.6 $Wm^{-1}K^{-1}$, however, an "S" shaped dependence of the thermal conductivity on the temperature is observed leading to higher κ values above room temperature [24].

Recently, another crystal family of monoclinic (sp. gr. *P*2/*c*) divalent-metal monotungstates $M^{2+}WO_4$ (where M = Mg, Cu, Ni, Co, Fe, Zn, Mn or Cd) has attracted attention for doping with rare-earth ions (RE^{3+}) with laser applications [10,25,26]. Two examples of such host crystals are magnesium and zinc monotungstates, $MgWO_4$ [27] and $ZnWO_4$ [28], respectively. These crystals offer better thermo-mechanical properties in comparison with two above mentioned families of tungstates, in particular, higher thermal conductivity ($\langle\kappa\rangle$ = 8.7 $Wm^{-1}K^{-1}$ for $MgWO_4$ [29]) and weaker anisotropy of the thermal expansion [25], that is im-

portant for power scaling of lasers. The large RE^{3+} ions in the $M^{2+}WO_4$ crystals substitute for the smaller divalent-metal cations (e.g., Mg^{2+} or Zn^{2+}) via a heterovalent mechanism, so that the segregation coefficients K_{RE} of the RE^{3+} dopants between the crystals and the fluxes are typically well below 1, and large RE^{3+} doping concentrations are hardly achievable in these materials [26]. However, the differences in ionic radii and valence of the active ions and the host-forming cations promote enlarged Stark splitting of the RE^{3+} multiplets and inhomogeneous broadening of the absorption and emission bands [25,30].

So far, laser operation with RE^{3+}-doped $MgWO_4$ crystals has been demonstrated at ~1 μm (with Yb^{3+}) [5,10] and at ~2 μm (with Tm^{3+} and Ho^{3+}) [25,31,32]. In the first report on Yb:$MgWO_4$, the crystal growth by the TSSG method, room-temperature (RT) spectroscopy and preliminary laser experiment were described [10]. Later on, low temperature (LT) spectroscopy and highly-efficient laser operation were reported: a diode-pumped 1.25 at.% Yb:$MgWO_4$ laser generated 18.2 W at ~1056 nm with a slope efficiency of 89% and a linearly polarized output [5]. In [33], an Yb:$MgWO_4$ oscillator was mode-locked by a SEmiconductor Saturable Absorber Mirror (SESAM) delivering 125 fs pulses at 1065 nm with a repetition rate of 117 MHz. In [34], a diode-pumped Yb:$MgWO_4$ laser generated an optical vortex beam corresponding to the first-order Laguerre–Gaussian doughnut beam (LG_{01}).

Compared to the research on RE^{3+}-doped $MgWO_4$ crystals for laser applications, much less attention has been paid to their zinc counterparts. However, unlike $MgWO_4$, $ZnWO_4$ crystals melt congruently at 1486 K and thus they can be easily grown by the conventional Czochralski (Cz) method [35,36]. The thermal conductivity of undoped $ZnWO_4$ is slightly higher than that for monoclinic double tungstates ($<\kappa>$ up to 4.3 $Wm^{-1}K^{-1}$) [24,37]. Undoped $ZnWO_4$ is well-known during many years as a promising scintillating material [35,36]. So far, one group repetitively presented the results on the growth and brief optical characterization of $ZnWO_4$ crystals doped with Yb^{3+}, Tm^{3+}, Er^{3+}, Ho^{3+} and Dy^{3+} [38-42]. Yang reported on laser operation of Yb:$ZnWO_4$ yielding 0.5 W at 1017 nm with an estimated slope efficiency of only ~6% [38]. Tm:$ZnWO_4$ and Dy:$ZnWO_4$ lasers are also known [43,44].

In the present work, we assess the potential of Yb^{3+}-doped zinc tungstate as a promising laser material at ~1 μm. The polarized room temperature (RT, 293 K) and low temperature (LT, down to 6 K) spectroscopy of Yb^{3+},Li^{+}:$ZnWO_4$ crystals are studied and efficient diode-pumped laser operation is achieved. In the first part of this work [45], we presented the results on the Cz crystal growth, its coloration, structure refinement and vibronic properties.

2. Experimental

2.1. Crystal growth

For spectroscopic and laser studies, two $ZnWO_4$ crystals codoped with (5 at.% Yb^{3+}, 5 at.% Li^{+}) and (3 at.% Yb^{3+}, 3 at.% Li^{+}) ions (nominal composition, in the growth charge) were grown by the Czochralski method. The growth was performed in Pt/Rh crucibles. The starting materials were WO_3, ZnO, Li_2CO_3 (as the source of Li^{+} ions) and Yb_2O_3. The Li^{+} ions were added as charge compensators of heterovalent Zn^{2+} to Yb^{3+} substitution. The starting composition was calculated assuming that the Yb^{3+} and Li^{+} ions substitute for the Zn^{2+} ones in the $ZnWO_4$ structure. For the growth, a [100]-oriented undoped seed was used. The

pulling rate was 1 mm/h and the rotation speed was 6 rpm. Once the growth was completed, the crystal was separated from the melt and slowly (at a rate of 8 K/h) cooled down to RT to avoid its cracking. The as-grown crystals were black-colored with a well-developed natural faceting parallel to the (010) cleavage plane. The crystals were oriented by means of the single-crystal X-ray diffraction. The crystal exhibited cleavage on the (010) plane.

The crystal coloration was removed by oxidizing annealing at a temperature of 800 °C. The duration at the maximum temperature was 24 hours. After annealing, thin (few mm) crystal plates became transparent having a weak rose coloration. More details about the crystal growth, cleavage, coloration and the ways of its removal can be found in the parallel paper [45].

The actual Yb^{3+} concentration N_{Yb} in the crystals was measured by the microprobe analysis using a Cameca Camebax SX-100 analyzer. It amounted to $N_{Yb} = 2.0\pm0.7\times10^{20}$ cm^{-3} (~1.4 at.% Yb) and $2.7\pm0.5\times10^{20}$ cm^{-3} (~1.8 at.% Yb) for the crystals with the nominal doping level of 3 at.% and 5 at.% Yb^{3+}, respectively.

2.2. Optical spectroscopy

The polarized RT absorption spectra were measured using a Varian CARY-5000 spectrophotometer and a Glan-Taylor polarizer. To measure the absorption spectra at LT, the sample was fixed within an Oxford Instruments Ltd. cryostat (model SU 12) with helium-gas close-cycle flow. The spectral bandwidth (SBW) was 0.6 nm.

The polarized RT (293 K) luminescence spectra were measured using an Ando AQ6315-E optical spectrum analyzer (OSA) and a Glan-Taylor polarizer. As an excitation source, we used a CW Ti:Sapphire laser tuned to 940 and 972 nm (the two measurments were combined to eliminate the excitation peak). For the LT studies, a Yokogawa AQ6373 OSA was employed using a 965 nm InGaAs laser diode as a pump source. The same cryostat was used.

The luminescence decay of Yb^{3+}:$ZnWO_4$ at ~1030 nm was studied using a 1/4 m monochromator (Oriel 77200), an InGaAs detector and a 300 MHz digital oscilloscope (TDS 3032B, Tektronix). The luminescence was excited by the output of a ns optical parametric oscillator (OPO, Horizon, Continuum) tuned to 960 nm.

3. Optical spectroscopy

3.1. Optical indicatrix

According to the Rietveld refinement of the X-ray powder diffraction patterns (see Part I of this paper), Yb^{3+},Li^{+}:$ZnWO_4$ belongs to the monoclinic crystal class (sp. gr. $P2/c$ – C^4_{2h}, wolframite-type structure). The lattice constants for the 1.8 at.% Yb^{3+},Li^{+}:$ZnWO_4$ crystal are a = 4.702(2) Å, b = 5.718(6) Å, c = 4.930(4) Å and β = 90.713(5)° with Z=2 [45]. This crystal is optically biaxial [46]. Its optical properties are described in the frame of mutually orthogonal optical indicatrix axes, denoted as X, Y and Z. Note that, in general, no relation for the n_X, n_Y and n_Z refractive indices is placed. One axis is parallel to the 2-fold monoclinic axis (the crystallographic ***b***-axis) and the other two are located in the orthogonal ***a***-***c*** plane making certain angles with the crystallographic axes.

The dispersion of the principal refractive indices of undoped $ZnWO_4$ was studied in [47] yielding the following values at 1.0 μm: $n_p = 2.1299$, $n_m = 2.1447$ and $n_g = 2.2790$. Here, we use the notations for monoclinic laser crystals, where the optical indicatrix axes are labeled as N_p, N_m and N_g according to the relation between the refractive indices: $n_p < n_m < n_g$. If the intermediate refractive index (n_m) is nearer in magnitude to the smallest one (n_p) than to n_g, the crystal is biaxial positive which is the case of $ZnWO_4$. The optical axes are located in the N_p-N_g plane and the angle between them, containing N_g, is $2V_g < 45°$ (for $ZnWO_4$, $2V_g = 38.4°$ at 1.0 μm, and this crystal is quasi-uniaxial). Here, Vg is the angle between each of the optical axes and the N_g-axis.

There exists a discrepancy in the assignment between the (X, Y, Z) and (N_p, N_m, N_g) axes for $ZnWO_4$ in the literature. The only work where the axes are unambiguously assigned is [48]. We will follow their convention: the N_p axis is parallel to the ***b***-axis and the N_m and N_g ones are located in the ***a***-***c*** plane, Fig. 1. According to [48], the angle between the N_g-axis and the ***c***-axis $\rho = 11.93°$ (at the longest available wavelength of 0.69 μm), measured within the monoclinic angle β. This assignment is in agreement with the early paper of Spengler and O'Hara where the (X, Y, Z) notations for the optical indicatrix axes were used assuming that the authors followed the $n_X < n_Y < n_Z$ convention [46]. However, both these studies disagree with the repetitive publications on RE^{3+}-doped $ZnWO_4$ crystals published more recently [39,42].

An overview of the reported refractive indices for $ZnWO_4$ is shown in Fig. 2(a). The data from different authors agree well. The experimental data on the dispersion of the n_p, n_m and n_g refractive indices were fitted using a single-pole Sellmeier formula with an IR correction term [49]:

$$n_i^2(\lambda) = A_i + \frac{B_i\lambda^2}{\lambda^2 - C_i^2} - D_i\lambda^2, \quad (1)$$

Here, A_i - D_i are the Sellmeier coefficients, λ is the light wavelength [in μm], and $i = p, m, g$. The obtained best-fit Sellmeier curves are shown in Fig. 2(a) and the corresponding A_i - D_i coefficients are listed in Table 1. The average deviation between the experimental data and their fits is about 0.0002.

The optical bandgap of undoped $ZnWO_4$ E_g is 3.9-4.4 eV [50].

Similarly to other monoclinic tungstates [49], a rotation of the dielectric frame with the wavelength was determined for $ZnWO_4$ in the angular range of $\rho = 6.88° - 11.93°$ for wavelengths between 0.40 and 0.69 μm [48]. Slightly different values of the ρ angle can be found in the literature: Spengler and O'Hara specified $\rho = 9.80°$ at 0.59 μm [46] and Bond gave $\rho = 8.20°$ at ~1 μm [47]. The literature data on ρ are summarized in Fig. 2(b) while the data from Bond [47] are shifted along the vertical axis to correspond to two other sources. They were fitted with the following formula [49]:

$$\rho(\lambda) = A + \frac{B}{\lambda} + \frac{C}{\lambda^2}, \quad (2)$$

where ρ is expressed in deg and λ is in μm. The best-fitting parameters $A = 12.792$ deg (it corresponds to the rotation angle in the long-wavelength limit, $\lambda \to \infty$), $B = 1.0294$ deg×μm

and C = -1.4239 deg×μm^2. At ~1 μm relevant for the Yb^{3+} ion, Eq. (2) gives ρ = 12.40°. This value is indicated in Fig. 1.

3.2. RT absorption cross-sections

The transition cross-sections were determined at RT using a 1.8 at.% Yb^{3+},Li^+:$ZnWO_4$ crystal ($N_{Yb} = 2.7\times10^{20}$ cm^{-3}).

The absorption cross-sections were calculated from the measured absorption coefficient, $\sigma^i_{abs} = \alpha^i_{abs}/N_{Yb}$ (where $i = N_p$, N_m, N_g is the light polarization). The results are shown in Fig. 3(a). The maximum $\sigma_{abs} = 2.40\times10^{-20}$ cm^2 at 972.7 nm and the corresponding full width at half maximum (FWHM) of the absorption peak is 8.3 nm (for light polarization $\boldsymbol{E} \parallel N_g$). This absorption peak corresponds to the zero-phonon line (ZPL) at RT (see below). The Yb^{3+},Li^+:$ZnWO_4$ crystal exhibits a notable anisotropy of the absorption cross-sections, as expressed by the ratios $\sigma_{abs}(N_g) : \sigma_{abs}(N_p) = 2.6 : 1$ and $\sigma_{abs}(N_g) : \sigma_{abs}(N_m) = 4.7 : 1$ at the wavelength of ~970 nm. Another intense and slightly broader absorption peak occurs at 958.4 nm ($\sigma_{abs} = 1.84\times10^{-20}$ cm^2 and FWHM = 9.8 nm again for $\boldsymbol{E} \parallel N_g$). Both absorption peaks are suitable for pumping with InGaAs laser diodes. Due to the broad absorption lines, Yb^{3+},Li^+:$ZnWO_4$ lasers are expected to be less sensitive to the temperature drift of the diode wavelength.

Compared to its magnesium counterpart (Yb^{3+}:$MgWO_4$ [5], for which $\sigma_{abs} = 6.16\times10^{-20}$ cm^2 at 974.0 nm with FWHM = 5.6 nm for $\boldsymbol{E} \parallel N_g$), the studied material exhibits lower peak absorption cross-section values whilst much broader absorption peaks. This effect is even more pronounced when comparing with the monoclinic double tungstate crystal Yb^{3+}:$KLu(WO_4)_2$ [8] (for which σ_{abs} is as high as 11.8×10^{-20} cm^2 at 981.0 nm with a FWHM of only 3.5 nm for the light polarization $\boldsymbol{E} \parallel N_m$).

In a previous work on Yb^{3+}:$ZnWO_4$ (without Li^+), a maximum absorption cross-section of 2.6×10^{-20} cm^2 at ~972 nm was reported [38]. This agrees with the present results. However, due to the probable confusion with the optical orientation of the sample, it is difficult to compare the polarized absorption spectra with those from [38].

3.3. RT stimulated-emission and gain cross-sections

The stimulated-emission (SE) cross-sections, σ_{SE}, were determined from the measured luminescence spectra for polarized light calibrated for the spectral response of the set-up using the Füchtbauer–Ladenburg (F-L) equation [51]:

$$\sigma^i_{SE}(\lambda) = \frac{\lambda^5}{8\pi\langle n\rangle^2 \tau_{rad} c} \frac{W_i(\lambda)}{(1/3)\sum_{i=p,m,g}\int \lambda W_i(\lambda)\mathrm{d}\lambda}, \quad (3)$$

where, λ is the light wavelength, $\langle n\rangle$ = 2.184 is the mean refractive index at the mean emission wavelength $\langle\lambda_{lum}\rangle$ = 1010.0 nm, c is the speed of light, τ_{rad} = 0.37 ms is the radiative lifetime of the emitting state ($^2F_{5/2}$), see below, and $W_i(\lambda)$ is the luminescence spectrum for i-th polarization ($i = p$, m, g). To avoid the unwanted effect of reabsorption on the measured luminescence spectra, thin (thickness: t <100 μm) (010)-oriented cleaved plates of Yb^{3+},Li^+:$ZnWO_4$ were used. The results are shown in Fig. 3(b).

The SE cross-sections can be calculated alternatively by the reciprocity method (RM), or McCumber equation [52,53]:

$$\sigma_{\mathrm{SE}}^{i}(\lambda)=\sigma_{\mathrm{abs}}^{i}(\lambda)\frac{Z_1}{Z_2}\exp\left(-\frac{(hc/\lambda)-E_{\mathrm{ZPL}}}{kT}\right), \tag{4}$$

where h is the Planck constant, (hc/λ) is the photon energy (in cm^{-1}), k is the Boltzmann constant, T is the crystal temperature (RT), E_{ZPL} is energy of the ZPL transition, and Z_m are the partition functions of the lower (m = 1) and upper (m =2) manifolds:

$$Z_m=\sum_k g_k^m \exp(-E_k^m/kT)\,. \tag{5}$$

Here, $g^m_k = 1$ is the degeneracy of the sub-level with the number k and energy E^m_k measured from the lowest sub-level of each multiplet.

Using the crystal-field splitting for the Yb^{3+} ion in $ZnWO_4$ (see Section 4.5), we calculated the SE cross-sections via Eq. (4). A comparison of the results obtained with the F-L equation and the RM for the light polarization $\boldsymbol{E} \parallel N_p$ is shown in Fig. 3(b). Note that due to the exponential term in Eq. (4), the precision of the SE cross-sections calculated by the RM is lower at longer wavelengths. The two methods used give a satisfactory agreement indicating the correctness of the selected τ_{rad} value (0.37±0.02 ms), as well as the weak influence of the reabsorption on the measured luminescence spectra.

The maximum $\sigma_{\mathrm{SE}} = 2.81\times10^{-20}$ cm^2 at 1055.6 nm and the corresponding emission bandwidth $\Delta\lambda_{\mathrm{em}}$ (FWHM) is ~12 nm (for $\boldsymbol{E} \parallel N_p$). Similarly to the absorption transition, strong anisotropy of the SE cross-sections is observed, namely $\sigma_{\mathrm{SE}}(N_p) : \sigma_{\mathrm{SE}}(N_g) = 4.6 : 1$ and $\sigma_{\mathrm{SE}}(N_p) : \sigma_{\mathrm{SE}}(N_m) = 6.2 : 1$ at ~1.06 μm. This will determine a linearly polarized output in the Yb^{3+},Li^+:$ZnWO_4$ lasers. Note that at the wavelength of ~973 nm (ZPL at RT in emission), the relation for the SE cross-sections is different, $\sigma_{\mathrm{SE}}(N_g) > \sigma_{\mathrm{SE}}(N_p) > \sigma_{\mathrm{SE}}(N_m)$, i.e., in agreement with the one discussed in Section 4.3. There exists another broader peak in the σ_{SE} spectra centered at 1004.1 nm featuring a FWHM of ~28 nm (again for $\boldsymbol{E} \parallel N_p$). The two other polarizations ($\boldsymbol{E} \parallel N_g$ and $\boldsymbol{E} \parallel N_m$) feature broader emission bandwidths at >1 μm, however, the spectra are rather structured. Thus, direct laser studies are needed to determine the optimum polarization for generation of ultrashort pulses in ML operation.

The peak σ_{SE} values in Yb^{3+},Li^+:$ZnWO_4$ are lower than those for its magnesium counterpart (Yb^{3+}:$MgWO_4$ [5], for which σ_{SE} reaches 6.2×10^{-20} cm^2 at 1056.7 nm for $\boldsymbol{E} \parallel N_m$ and the emission bandwidth $\Delta\lambda_{\mathrm{em}}$ (FWHM) is 19 nm) and similar to the SE cross-sections for monoclinic double tungstate Yb^{3+}:$KLu(WO_4)_2$ (for which $\sigma_{\mathrm{SE}} = 2.64\times10^{-20}$ cm^2 at 1026.6 nm and $\Delta\lambda_{\mathrm{em}}$ is ~10 nm [8]. The emission bandwidth for Yb^{3+},Li^+:$ZnWO_4$ is similar or even better than in the two above mentioned tungstate crystals. Note that here, we consider the SE cross-sections at wavelengths longer than the ZPL since such wavelengths are typically expected in bulk Yb lasers (see below).

The Yb^{3+} ion represents a quasi-three-level laser scheme with reabsorption at the laser wavelength. Thus, the gain cross-sections:

$$\sigma_{\mathrm{gain}} = \beta\sigma_{\mathrm{SE}} - (1-\beta)\sigma_{\mathrm{abs}},\,. \tag{6}$$

where $\beta = N_2(^2F_{5/2})/N_{Yb}$ is the inversion ratio and N_2 is the population of the upper laser level ($^2F_{5/2}$), are calculated to conclude about the possible laser wavelength and gain bandwidths $\Delta\lambda_{gain}$. The results are shown in Fig. 4 for the high-gain light polarizations $\boldsymbol{E} \parallel N_p$ and $\boldsymbol{E} \parallel N_g$. For $\boldsymbol{E} \parallel N_p$, the local peak at ~1056 nm dominates in the gain spectra. The gain bandwidth $\Delta\lambda_{gain}$ (FWHM) is 11.6 nm (for $\beta = 0.15$). For the $\boldsymbol{E} \parallel N_g$ polarization, with increasing the inversion ratio, several local maxima in the gain spectra are observed at ~1056, 1040, 1022 and 1003 nm. The gain bandwidth is larger, $\Delta\lambda_{gain} = 22.2$ nm (for the same $\beta = 0.15$).

Note that the strongest emission peak of Yb^{3+} ions in the Yb^{3+},Li^+:$ZnWO_4$ crystal (at the wavelength of ~1056 nm for $\boldsymbol{E} \parallel N_p$) corresponds to almost zero absorption (the reabsorption cross-section, $\sigma_{abs} = 0.05\times10^{-20}$ cm^2). This causes positive gain around this wavelength even at low β, that gives a hope for obtaining low threshold lasing at ~1056 nm in the Yb^{3+},Li^+:$ZnWO_4$ crystal.

3.4. Luminescence decay

The luminescence decay of Yb^{3+},Li^+:$ZnWO_4$ was studied at RT. Very thin (t <100 μm) cleaved plates were used to avoid the radiation trapping effect. The decay curve, Fig. 5, is single-exponential and the luminescence lifetime τ_{lum} is 367 μs. This agrees with the presence of a single site for Yb^{3+} ions in $ZnWO_4$ (symmetry: C_2). Previously for Yb^{3+}:$ZnWO_4$ (without Li^+ codoping), τ_{lum} was determined to be 644 μs using a bulk crystal [38]. This value may be overestimated due to the reabsorption effect.

The calculation of the SE cross-sections by two independent methods (the F-L equation and the RM, Section 3.3), yields an estimation for the radiative lifetime $\tau_{rad} = 0.37\pm0.02$ ms. Thus, the luminescence quantum efficiency for Yb^{3+},Li^+:$ZnWO_4$ $\eta_q = \tau_{lum}/\tau_{rad}$ is close to unity. This agrees with the "energy-gap law" for non-radiative relaxation [54] postulating that it is weak when the energy-gap to the lower-lying multiplet ($\Delta E = 9481$ cm^{-1}, in our case) is at least 4 times higher than the maximum phonon energy of the host ($h\nu_{ph} = 906$ cm^{-1} [45]).

3.5. Crystal-field splitting

To resolve the Stark splitting of the Yb^{3+} multiplets in $ZnWO_4$, the polarized absorption and luminescence spectra were measured in the temperature range of 6–293 K, Fig. 6. The studies were performed for the following light polarizations: $\boldsymbol{E} \parallel \boldsymbol{a}$ ($\approx N_m$) and $\boldsymbol{E} \parallel \boldsymbol{b}$ (N_p) in absorption and $\boldsymbol{E} \parallel \boldsymbol{c}$ ($\approx N_g$) and $\boldsymbol{E} \parallel \boldsymbol{b}$ (N_p) in emission. For Yb^{3+} ions in sites with the C_2 symmetry, there is a total of $J + 1/2$ Stark sub-levels for each $^{2S+1}L_J$ multiplet, denoted as 0..3 for $^2F_{7/2}$ and 0'..2' for $^2F_{5/2}$, respectively. The interpretation of the electronic transitions was performed accounting for the Raman spectra (see Part I of this paper).

At the temperature of 6 K, the populations of all the Stark sub-levels of the ground multiplet (except of the lowest one) are greatly reduced. Moreover, the electron-phonon coupling is also suppressed. Nevertheless, Yb^{3+} ions in $ZnWO_4$ exhibit large bandwidth of the zero-phonon line (ZPL), i.e., the transition between the lowest Stark sub-levels of two multiplets, or 0 ↔ 0'. Indeed, $\Delta\lambda_{ZPL} = 3.0$ nm (for $\boldsymbol{E} \parallel N_p$, as determined from the luminescence spectrum measured with a better resolution of SBW = 0.6 nm). Compared to the monoclinic Yb:$KY(WO_4)_2$ crystal ($\Delta\lambda_{ZPL}$ <0.1 nm for $\boldsymbol{E} \parallel N_p$) [55], this is much broader. Besides that, the

ZPL in absorption has a poorly resolved slightly asymmetric shape. The notable inhomogeneous broadening of the ZPL transition in the Yb^{3+},Li^{+}:$ZnWO_4$ crystal can be explained both by the difference in the ionic radii of Yb^{3+}, Li^{+} and Zn^{2+} ions (R_{Yb} = 0.868 Å, R_{Li} = 0.76 Å and R_{Zn} = 0.74 Å for VI-fold oxygen coordination [56]), and by heterovalent mechanism of substitution of Zn^{2+} by Yb^{3+} and Li^{+} ions.

Formally, $ZnWO_4$ is an ordered crystal; the Zn^{2+} ions accommodate in a single type of sites (Wyckoff symbol: 2*e*). However, in reality, each Li^{+}, and, especially, Yb^{3+} ion in the Zn^{2+} sub-lattice is a charged point defect, which brings both the spatial distortions (due to the difference in ionic radii), and the distortions in distribution of the electron density (due to the difference in formal charges) in its local environment. Besides that, as it was shown in the first part of this work [45], the actual Li^{+} amount in the crystal is lower than the content of Yb^{3+} ions. It means that essential part of Yb^{3+} remains uncompensated by Li^{+} ions. Thus, there additionally should be some amount of another kind charge compensators, probably, zinc vacancies. It is the third kind of point defects, acting in a similar way, as Yb^{3+} and Li^{+} ions do. Each Yb^{3+} active center has its own kind of surrounding by these three kinds of points defects, and, consequently, its own kind of crystal field, very slightly differing from that of other Yb^{3+} active centers. In other words, some (rather slight) extent of the structural disordering do exist in the crystal. A similar behavior was detected recently for Yb^{3+}-doped isostructural $MgWO_4$ crystal, revealing $\Delta\lambda_{ZPL}$ = 3.3 nm for $\boldsymbol{E} \parallel N_m$ [5].

The energy-level scheme of Yb^{3+} in $ZnWO_4$ is shown in Fig. 7(a). The ZPL has an energy of E_{ZPL} = 10285 cm^{-1}. The corresponding transition wavelength at 6 K is 972.3 nm. At RT, the partition functions Z_m for the lower (m = 1) and upper (m =2) manifolds are Z_1 = 1.345 and Z_2 = 1.548 (the ratio: Z_1/Z_2 = 0.869).

The total Stark splitting of the ground-state $\Delta E(^2F_{7/2})$ is 804 cm^{-1}. In general, larger $\Delta E(^2F_{7/2})$ supports wavelength tuning, shorter pulses under ML operation regime, longer achievable laser wavelengths, as well as lower lasing threshold and its weaker sensitivity to the temperature increase. The ground-state splitting for Yb^{3+} in $ZnWO_4$ exceeds those of other known tungstate crystals employed for diode-pumped lasers at ~1 μm, such as monoclinic ordered Yb:$MgWO_4$, 765 cm^{-1} [5], monoclinic ordered Yb:$KLu(WO_4)_2$, 559 cm^{-1} [8], and tetragonal disordered Yb:$NaGd(WO_4)_2$, 482 cm^{-1} (2*d* sites) and 492 cm^{-1} (2*b* sites) [22], Fig. 7(b). Note that the local symmetry of the site (sites) for Yb^{3+} ions is the same for all the considered monoclinic crystals (C_2) and it is different for the tetragonal scheelite-type one (S_4).

For all the RE^{3+} ions, it is known that the barycenter energy of any isolated $^{2S+1}L_J$ $4f^n$ multiplet shows a linear variation with the barycenter energy of any other multiplet. This is expressed by the so-called barycenter plot [57], Fig. 8. The barycenter energies $<E(^2F_{5/2})>$ and $<E(^2F_{7/2})>$ for Yb^{3+},Li^{+}:$ZnWO_4$ agree well with the linear fit of this plot, expressed by the equation $E(^2F_{5/2}) = 10166.6 + 0.997 \times E(^2F_{7/2})$ [in cm^{-1}], where E_0 = 10166.6 cm^{-1} has the meaning of the energy of the Yb^{3+} excited-state assuming a free ion. This analysis confirms the correctness of the constructed energy-level scheme.

4. Laser operation

4.1. Laser set-up

For laser experiments, we fabricated a rectangular active element from the 1.8 at.% Yb^{3+},Li^{+}:$ZnWO_4$ crystal (t = 3.85 mm, aperture: 7.3×6.5 mm^2). It was cut for light propagation along the ***a***-axis (***a***-cut). Its input and output facets were polished to laser quality and remained uncoated. The element was wrapped with In foil from all four lateral sides to improve the thermal contact and mounted in a Cu-holder. The latter was cooled by circulating water (T = 12 °C). The laser crystal was placed in a linear plano-concave (hemispherical) cavity formed by a flat pump mirror (PM) coated for high transmission (HT) at the pump wavelength (~0.97 μm) and for high reflectance (HR) at 1.02–1.2 μm, and a set of concave output couplers (OCs) with a transmission T_{OC} = 3%-10% at the laser wavelength (~1.06 μm) and a radius of curvature (RoC) of 50 mm, Fig. 9. The PM was placed at ~1 mm separation from the laser element. The geometrical cavity length was 49 mm.

The pump source was a fiber-coupled (N.A. = 0.22, fiber core diameter: 105 μm) InGaAs laser diode emitting up to 54 W of unpolarized output at a central wavelength of 968 nm (emission bandwidth: 1.5 nm, $M^2 \approx 37$). The pump was reimaged into the crystal using a lens assembly (imaging ratio: 1:1, f = 30 mm) leading to a pump spot diameter $2w_P \approx 100$ μm and a confocal parameter $2z_R \approx 1$ mm (in the crystal). Despite the reflectivity of the OCs at the pump wavelength, the counter-propagating pump beam was focused before the crystal, so that the second pass of the pump did not contribute to the laser output. The small-signal pump absorption η_{abs0} was calculated from the unpolarized transmission spectrum to be 32.8%. The value determined from the pump-transmission measurement at the threshold pump power and accounting for the absorption saturation was smaller, $\eta_{abs,L}$ = 23.2%. It was used to determine the absorbed pump power, P_{abs}. Here, we took into account the Fresnel losses at the uncoated crystal surfaces.

4.2. Laser performance

The Yb^{3+},Li^{3+}:$ZnWO_4$ laser generated a maximum output power of 2.90 W at ~1059 nm with a slope efficiency η = 57.9% (with respect to the absorbed pump power) and a laser threshold P_{th} of 0.41 W, Fig. 10(a). The optical-to-optical efficiency η_{opt} (vs. the pump power incident on the crystal) reached 11.2% (all the values are specified for T_{OC} = 10%). For smaller output coupling transmission, the slope efficiency was inferior while the laser threshold slightly decreased (η = 41.5% and P_{th} = 0.29 W for T_{OC} = 3%). For all OCs, a thermal roll-over in the input-output dependences was observed for P_{abs} > 5 W and assigned to non-optimized cooling of the laser element.

The laser emission was linearly polarized (***E*** || N_p), the polarization was naturally selected by the gain anisotropy. The emission spectra, Fig. 10(b), were weakly dependent on the output coupling being an interesting advantage. The laser operated around 1.06 μm in agreement with the gain spectra, Fig. 4(a).

In a previous study of a 1.25 at.% Yb:$MgWO_4$ crystal in the hemispherical cavity under diode pumping, the laser performance was similar: 2.52 W at ~1060 nm with η = 61% (*vs.* P_{abs}) [10]. However, the laser threshold was higher than in our case, P_{th} = 0.97 W. Note that much better CW laser performance was achieved with a microchip Yb:$MgWO_4$ laser [5] be-

cause of the optimized dimensions of the crystal leading to its efficient cooling and good mode-matching efficiency determined by the positive thermal lens.

No thermal fracture of the crystal was observed up to at least P_{abs} of 6 W. It is known that $M^{2+}WO_4$ crystals exhibit high thermal fracture limit [5].

5. Conclusions

To conclude, the Yb^{3+},Li^{+}:$ZnWO_4$ crystal is promising for ~1 μm lasers since it combines (i) good thermal properties (high thermal conductivity and weak anisotropy of thermal expansion) enabling power scaling, (ii) intense spectral bands with polarized light leading to linearly polarized laser emission, (iii) broad emission bands and large total Stark splitting of the ground-state ($^2F_{7/2}$) - largest among other Yb^{3+}-doped tungstate laser crystals and (iv) weak reabsorption at the laser wavelength. The attractive spectroscopic properties of Yb^{3+},Li^{+}:$ZnWO_4$ are attributed to the low symmetry of the Yb^{3+} site (C_2) and inhomogeneous broadening arising from the difference in the valence and ionic radius of the cations participating in the doping mechanism (Yb^{3+}, Li^{+} and Zn^{2+}). Some of the above characteristics make Yb^{3+},Li^{+}:$ZnWO_4$ very attractive for tunable and ML lasers as well as ultrafast amplifiers.

We report on efficient diode-pumped RT laser operation of a 1.8 at.% Yb^{3+},Li^{+}:$ZnWO_4$ crystal generating multi-watt output with a slope efficiency of 57.9%. This result well overcomes the previous report (which, in addition, was not supported by the laser power transfer characteristics) [38], proving that Yb^{3+}-doped zinc tungstate is an efficient laser material.

Regarding CW laser operation, further power scaling and improvement of the slope efficiency are possible. One direction of research to reach this goal is the elimination of the residual (rose) crystal coloration, e.g., by using Pt crucibles and high-purity reagents during the crystal growth. Another important issue is the control of the charge compensation during Yb^{3+} doping, e.g., by introducing larger amount of Li^{+} cations or by using other ions (Na^{+}, Nb^{5+}). This may help to improve the segregation coefficient of Yb^{3+} ions in $ZnWO_4$ leading to higher achievable doping levels and, thus, better pump absorption efficiency. The design of the laser cavity for diode-pumped Yb^{3+},Li^{+}:$ZnWO_4$ lasers requires additional knowledge about the thermo-optical properties, such as the dn/dT coefficients and thermal lensing.

Due to its broad transparency, $ZnWO_4$ is also promising for doping with other RE^{3+} ions such as Tm^{3+} or Ho^{3+} for laser operation in the spectral range of ~2 μm.

Acknowledgements

This work was supported by the Spanish Government (project No. MAT2016-75716-C2-1-R (AEI/FEDER,UE)) and by Generalitat de Catalunya (project No. 2017SGR755). It was funded by the Russian Foundation for Basic Research (RFBR, grant No. 18-02-01058). It was co-financed by the European Regional Development Fund and the state budget of the Czech Republic (project HiLASE CoE: Grant No. CZ.02.1.01/0.0/0.0/15_006/0000674) and by the European Union's Horizon 2020 research and innovation programme under grant agreement No. 739573. This work was also supported by the Ministry of Education, Youth and Sports of the Czech Republic (Programm NPU I Project No. LO1602).

References

1. J. Liu, V. Petrov, H. Zhang, J. Wang, Power scaling of a continuous-wave and passively Q-switched Yb:$KLu(WO_4)_2$ laser end-pumped by a high-power diode, Appl. Phys. B 88 (2007) 527–530.

2. J. M. Serres, V. Jambunathan, P. Loiko, X. Mateos, H. Yu, H. Zhang, J. Liu, A. Lucianetti, T. Mocek, K. Yumashev, U. Griebner, V. Petrov, M. Aguiló, F. Díaz, Microchip laser operation of Yb-doped gallium garnets, Opt. Mater. Express 6 (2016) 46-57.

3. J. Liu, V. Petrov, H. Zhang, J. Wang, M. Jiang, High-power laser performance of *a*-cut and *c*-cut Yb:$LuVO_4$ crystals, Opt. Lett. 31 (2006) 3294-3296.

4. P. Loiko, J. M. Serres, X. Mateos, X. Xu, J. Xu, V. Jambunathan, P. Navratil, A. Lucianetti, T. Mocek, X. Zhang, U. Griebner, V. Petrov, M. Aguiló, F. Díaz, A. Major, Microchip Yb:$CaLnAlO_4$ lasers with up to 91% slope efficiency, Opt. Lett. 42 (2017) 2431-2434.

5. P. Loiko, M. Chen, J.M. Serres, M. Aguiló, F. Díaz, H. Lin, G. Zhang, L. Zhang, Z. Lin, P. Camy, S. B. Dai, Z. Chen, Y. Zhao, L. Wang, W. Chen, U. Griebner, V. Petrov, X. Mateos, Spectroscopy and high-power laser operation of a monoclinic Yb^{3+}:$MgWO_4$ crystal, Opt. Lett. 45 (2020) 1770-1773.

6. U. Griebner, S. Rivier, V. Petrov, M. Zorn, G. Erbert, M. Weyers, X. Mateos, M. Aguiló, J. Massons, F. Díaz, Passively mode-locked Yb:$KLu(WO_4)_2$ oscillators, Opt. Express 13 (2005) 3465–3470.

7. F. Auzel, D. Meichenin, F. Pelle, P. Goldner, Cooperative luminescence as a defining process for RE-ions clustering in glasses and crystals, Opt. Mater. 4 (1994) 35-41.

8. V. Petrov, M. C. Pujol, X. Mateos, Ò. Silvestre, S. Rivier, M. Aguiló, R. M. Solé, J. H. Liu, U. Griebner, F. Díaz, Growth and properties of $KLu(WO_4)_2$, and novel ytterbium and thulium lasers based on this monoclinic crystalline host, Laser Photon. Rev. 1 (2007) 179-212.

9. A. García-Cortés, J. M. Cano-Torres, M. D. Serrano, C. Cascales, C. Zaldo, S. Rivier, X. Mateos, U. Griebner, V. Petrov, Spectroscopy and lasing of Yb-doped $NaY(WO_4)_2$: tunable and femtosecond mode-locked laser operation, IEEE J. Quantum Electron. 43 (2007) 758-764.

10. L. Zhang, W. Chen, J. Lu, H. Lin, L. Li, G. Wang, G. Zhang, Z. Lin, Characterization of growth, optical properties, and laser performance of monoclinic Yb:$MgWO_4$ crystal, Opt. Mater. Express 6 (2016) 1627-1634.

11. K.A. Subbotin, E.V. Zharikov, V.A. Smirnov, Yb-and Er-doped single crystals of double tungstates $NaGd(WO_4)_2$, $NaLa(WO_4)_2$, and $NaBi(WO_4)_2$ as active media for lasers operating in the 1.0 and 1.5 μm ranges, Opt. Spectr. 92 (2002) 601-608 [transl. from Optika i Spektroskopiya 92 (2002) 657–664].

12. J. Liu, U. Griebner, V. Petrov, H. Zhang, J. Zhang, J. Wang, Efficient continuous-wave and Q-switched operation of a diode-pumped Yb:$KLu(WO_4)_2$ laser with self-Raman conversion, Opt. Lett. 30 (2005) 2427-2429.

13. A. A. Lagatsky, N. V. Kuleshov, V. P. Mikhailov, Diode-pumped CW lasing of Yb:KYW and Yb:KGW, Opt. Commun. 165 (1999) 71-75.

14. P. A. Loiko, V. E. Kisel, N. V. Kondratuk, K. V. Yumashev, N. V. Kuleshov, A. A. Pavlyuk, 14 W high-efficiency diode-pumped cw Yb:$KGd(WO_4)_2$ laser with low thermo-optic aberrations, Opt. Mater. 35 (2013) 582– 585.

15. J. M. Serres, P. Loiko, X. Mateos, K. Yumashev, N. Kuleshov, V. Petrov, U. Griebner, M. Aguiló, F. Díaz, Prospects of monoclinic Yb:KLu(WO_4)$_2$ crystal for multi-watt microchip lasers, Opt. Mater. Express 5 (2015) 661–667.
16. P. Loiko, J. M. Serres, X. Mateos, K. Yumashev, A. Yasukevich, V. Petrov, U. Griebner, M. Aguiló, F. Díaz, Sub-nanosecond Yb:KLu(WO_4)$_2$ microchip laser, Opt. Lett. 41 (2016) 2620–2623.
17. S. Pekarek, C. Fiebig, M. C. Stumpf, A. E. H. Oehler, K. Paschke, G. Erbert, T. Südmeyer, U. Keller, Diode-pumped gigahertz femtosecond Yb:KGW laser with a peak power of 3.9 kW, Opt. Express 18 (2010) 16320–16326.
18. O. Silvestre, J. Grau, M. C. Pujol, J. Massons, M. Aguiló, F. Díaz, M. T. Borowiec, A. Szewczyk, M. U. Gutowska, M. Massot, A. Salazar, V. Petrov, Thermal properties of monoclinic KLu(WO_4)$_2$ as a promising solid state laser host, Opt. Express 16 (2008) 5022–5034.
19. P. A. Loiko, K. V. Yumashev, N. V. Kuleshov, G. E. Rachkovskaya, A. A. Pavlyuk, Detailed characterization of thermal expansion tensor in monoclinic KRe(WO_4)$_2$ (where Re = Gd, Y, Lu, Yb), Opt. Mater. 34 (2011) 23-26.
20. Y.K. Voron'ko, E.V. Zharikov, D.A. Lis, A.A. Sobol, K.A. Subbotin, S.N. Ushakov, V.E. Shukshin, Spectroscopic investigations of NaGd(WO_4)$_2$ and NaLa(MoO_4)$_2$ single crystals doped by Yb^{3+} ions, Proc. SPIE 5478 (2004) 60-68.
21. A. García-Cortés, C. Zaldo, C. Cascales, Site selective spectroscopy of Yb^{3+} in NaT(WO_4)$_2$, T = Bi, Gd, Y, Lu, laser crystals: Assessment with simulated crystal field effects, Opt. Mater. 31 (2009) 1096-1100.
22. C. Cascales, M. D. Serrano, F. Esteban-Betegón, C. Zaldo, R. Peters, K. Petermann, G. Huber, L. Ackermann, D. Rytz, C. Dupré, M. Rico, J. Liu, U. Griebner, V. Petrov, Structural, spectroscopic, and tunable laser properties of Yb^{3+}-doped NaGd(WO_4)$_2$, Phys. Rev. B 74 (2006) 174114.
23. Y.K. Voron'ko, E.V. Zharikov, D.A. Lis, K.A. Subbotin, S.N. Ushakov, V.E. Shukshin, S. Dröge, Growth and luminescent properties of NaGd(WO_4)$_2$:Yb^{3+} crystals, Inorg. Mater. 39 (2003) 1308-1314 [transl. from Neorganicheskie Materialy 39 (2003) 1509–1516].
24. M.D. Serrano, C. Cascales, X. Han, C. Zaldo, A. Jezowski, P. Stachowiak, N. Ter-Gabrielyan, V. Fromzel, M. Dubinskii, Thermal characterization, crystal field analysis and in-band pumped laser performance of Er doped NaY(WO_4)$_2$ disordered laser crystals, PLOS one 8 (2013) e59381.
25. L. Zhang, P. Loiko, J. M. Serres, E. Kifle, H. Lin, G. Zhang, E. Vilejshikova, E. Dunina, A. Kornienko, L. Fomicheva, U.Griebner, V. Petrov, Z. Lin, W. Chen, K. Subbotin, M. Aguiló, F. Díaz, X. Mateos, Growth, spectroscopy and first laser operation of monoclinic Ho^{3+}:$MgWO_4$ crystal, J. Lumin. 213 (2019) 316-325.
26. L. Zhang, H. Lin, G. Zhang, X. Mateos, J. M. Serres, M. Aguiló, F. Díaz, U. Griebner, V. Petrov, Y. Wang, P. Loiko, E. Vilejshikova, K. Yumashev, Z. Lin, W. Chen, Crystal growth, optical spectroscopy and laser action of Tm^{3+}-doped monoclinic magnesium tungstate, Opt. Express 25 (2017) 3682-3693.
27. L. Li, Y. Yu, G. Wang, L. Zhang, Z. Lin, Crystal growth, spectral properties and crystal field analysis of Cr^{3+}:$MgWO_4$, Cryst. Eng. Comm. 15 (2013) 6083-6089.
28. X. Wang, Z. Fan, H. Yu, H. Zhang, J. Wang, Characterization of $ZnWO_4$ Raman crystal, Opt. Mater. Express 7 (2017) 1732-1744.

29. L. Zhang, Y. Huang, S. Sun, F. Yuan, Z. Lin, G. Wang, Thermal and spectral characterization of Cr^{3+}:$MgWO_4$—a promising tunable laser material, J. Lumin. 169 (2016) 161-164.
30. P. Loiko, Y. Wang, J. M. Serres, X. Mateos, M. Aguiló, F. Díaz, L. Zhang, Z. Lin, H. Lin, G. Zhang, E. Vilejshikova, E. Dunina, A. Kornienko, L. Fomicheva, V. Petrov, U. Griebner, W. Chen, Monoclinic Tm^{3+}:$MgWO_4$ crystal: Crystal-field analysis, tunable and vibronic laser demonstration, J. Alloys Compd. 763 (2018) 581-591.
31. P. Loiko, J. M. Serres, X. Mateos, M. Aguiló, F. Díaz, L. Zhang, Z. Lin, H. Lin, G. Zhang, K. Yumashev, V. Petrov, U. Griebner, Y. Wang, S. Y. Choi, F. Rotermund, W. Chen, Monoclinic Tm^{3+}:$MgWO_4$: a promising crystal for continuous-wave and passively Q-switched lasers at ~2 μm, Opt. Lett. 42 (2017) 1177-1180.
32. Y. Wang, W. Chen, M. Mero, L. Zhang, H. Lin, Z. Lin, G. Zhang, F. Rotermund, Y. J. Cho, P. Loiko, X. Mateos, U. Griebner, V. Petrov, Sub-100 fs Tm:$MgWO_4$ laser at 2017 nm mode locked by a graphene saturable absorber, Opt. Lett. 42 (2017) 3076-3079.
33. H. Lin, G. Zhang, L. Zhang, Z. Lin, F. Pirzio, A. Agnesi, V. Petrov, W. Chen, Continuous-wave and SESAM mode-locked femtosecond operation of a Yb:$MgWO_4$ laser, Opt. Express 25 (2017) 11827-11832.
34. J. Lu, H. Lin, G. Zhang, B. Li, L. Zhang, Z. Lin, Y.F. Chen, V. Petrov, W. Chen, Direct generation of an optical vortex beam from a diode-pumped Yb:MgWO4 laser, Laser Phys. Lett. 14 (2017) 085807.
35. L. L. Nagornaya, A. M. Dubovik, Y. Y. Vostretsov, B. V. Grinyov, F. A. Danevich, K. A. Katrunov, V. M. Mokina, G. M. Onishchenko, D. V. Poda, N. G. Starzhinskiy, I. A. Tupitsyna, Growth of $ZnWO_4$ crystal scintillators for high sensitivity 2β experiments, IEEE Trans. Nucl. Sci. 55 (2008) 1469-1472.
36. E. N. Galashov, V. A. Gusev, V. N. Shlegel, Y. V. Vasiliev, The growth of $ZnWO_4$ and $CdWO_4$ single crystals from melt by the low thermal gradient Czochralski technique, Cryst. Rep. 54 (2009) 689-691 [transl. from Kristallografiya 54 (2009) 733–735].
37. P. A. Popov, S. A. Skrobov, A. V. Matovnikov, N. V. Mitroshenkov, Y. A. Borovlev, Thermal conductivity and heat capacity of a $ZnWO_4$ crystal, Phys. Solid State 58 (2016) 853-856 [transl. from Fizika Tverdogo Tela 58 (2016) 827–830].
38. F. Yang, The spectroscopic investigation of $ZnWO_4$:Yb^{3+} single crystal, J. Mater. Res. 27 (2012) 2096-2100.
39. F. Yang, C. Tu, J. Li, G. Jia, H. Wang, Y. Wei, Z. You, Z. Zhu, Y. Wang, X. Lu, Growth and optical property of $ZnWO_4$:Er^{3+} crystal, J. Lumin. 126 (2007) 623-628.
40. F. Yang, C. Tu, H. Wang, Y. Wei, Z. You, G. Jia, J. Li, Z. Zhu, X. Lu, Y. Wang, Growth and spectroscopy of Dy^{3+} doped in $ZnWO_4$ crystal, Opt. Mater. 29 (2007) 1861-1865.
41. F. Yang, C. Tu, H. Wang, Y. Wei, Z. You, G. Jia, J. Li, Z. Zhu, X. Lu, Y. Wang, Growth and spectroscopy of $ZnWO_4$:Ho^{3+} crystal, J. Alloys Compd. 455 (2008) 269-273.
42. F. Yang, C. Tu, The spectroscopy investigation of $ZnWO_4$:Tm^{3+} single crystal, J. Alloys Compd. 535 (2012) 83-86.
43. Z. Xia, F. Yang, L. Qiao, F. Yan, End pumped yellow laser performance of Dy^{3+}:$ZnWO_4$, Opt. Commun. 387 (2017) 357-360.
44. F.G. Yang, Z.Y. You, C.Y. Tu, End-pumping $ZnWO_4$:Tm^{3+} at ~1.9 μm eye-safe laser, Laser Phys. Lett. 9 (2012) 204-206.

45. K. Subbotin, P. Loiko, A. Volokitina, A. Titov, D. Lis, E. Chernova, S. Slimi, R.M. Solé, U. Griebner, V. Petrov, M. Aguiló, F. Díaz, X. Mateos, E. Zharikov, Monoclinic zinc monotungstate Yb^{3+},Li^{+}:$ZnWO_4$: Part I. Czochralski growth, structure refinement and Raman spectra, J. Lumin., *submitted* (2020).
46. C.J. Spengler, S. O'Hara, Zinc tungstate - some optical properties, Appl. Opt. 3 (1964) 1084-1085.
47. W.L. Bond, Measurement of the refractive indices of several crystals, J. Appl. Phys. 36 (1965) 1674-1677.
48. H. Wang, Y. Lin, Y.-D. Zhou, G. Chen, T. Zhou, J. H. Wang, B.-Q. Hu, Optical characteristics of $ZnWO_4$ single crystals, Acta Phys. Sinica 38 (1989) 670-674.
49. B. Zysset, I. Biaggio, P. Günter, Refractive indices of orthorhombic $KNbO_3$. I. Dispersion and temperature dependence, J. Opt. Soc. Am. B 9 (1992) 380-386.
50. R. Lacomba-Perales, J. Ruiz-Fuertes, D. Errandonea, D. Martínez-García, A. Segura, Optical absorption of divalent metal tungstates: correlation between the band-gap energy and the cation ionic radius, Europhys. Lett. 83 (2008) 37002.
51. B. Aull, H. Jenssen, Vibronic interactions in Nd:YAG resulting in nonreciprocity of absorption and stimulated emission cross sections, IEEE J. Quantum Electron. 18 (1982) 925-930.
52. D. E. McCumber, Einstein relations connecting broadband emission and absorption spectra, Phys. Rev. 136 (1964) A954–A957.
53. S. A. Payne, L. L. Chase, L. K. Smith, W. L. Kway, W. F. Krupke, Infrared cross-section measurements for crystals doped with Er^{3+}, Tm^{3+} and Ho^{3+}, IEEE J. Quantum Electron. 28 (1992) 2619-2630.
54. H. Scheife, G. Huber, E. Heumann, S. Bär, E. Osiac, Advances in up-conversion lasers based on Er^{3+} and Pr^{3+}, Opt. Mater. 26 (2004) 365-374.
55. E. Castellano-Hernández, X. Han, M. Rico, L. Roso, C. Cascales, C. Zaldo, Mode-locked laser operation of Indium-modified Yb:$KY(WO_4)_2$ single crystal, Opt. Express 23 (2015) 11135-11140.
56. R. D. Shannon, Revised effective ionic radii and systematic studies of interatomic distances in halides and chalcogenides, Acta Cryst. A 32 (1976) 751-767.
57. P. H. Haumesser, R. Gaumé, B. Viana, E. Antic-Fidancev, D. Vivien, Spectroscopic and crystal-field analysis of new Yb-doped laser materials, J. Phys.: Cond. Matter 13 (2001) 5427-5447.

List of figure captions

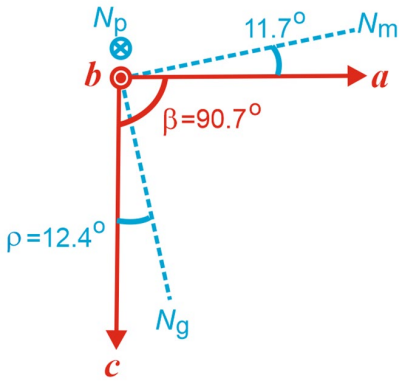

Figure 1. Orientation of the optical indicatrix axes (N_p, N_m, N_g) with respect to the crystallographic frame (***a***, ***b***, ***c***) in monoclinic $ZnWO_4$. The angle ρ is specified at the wavelength of ~1 μm.

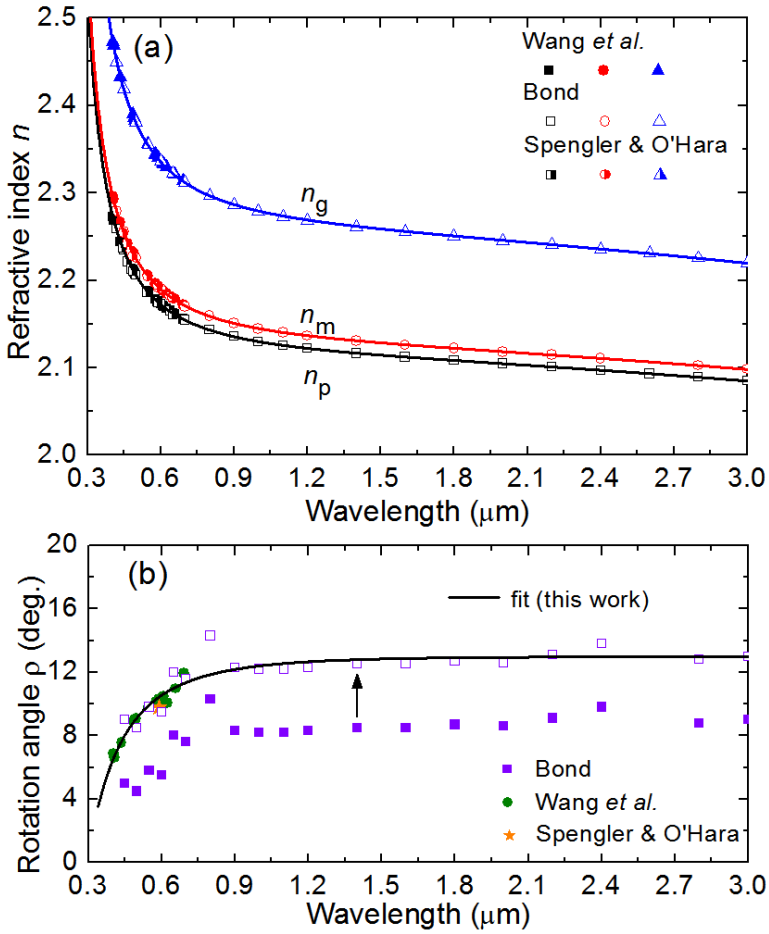

Figure 2. (a) Dispersion of the principal refractive indices (n_p, n_m, n_g) in monoclinic $ZnWO_4$: *symbols* – literature data [46-48], *curves* – their fitting using Eq. (1). The best-fit parameters are listed in Table 1; (b) rotation of the dielectric frame (expressed by the angle ρ between the N_g and ***c*** axes in the ***a***-***c*** plane, Fig. 1) as a function of wavelength, *symbols* – literature data [46-48], *curves* – their fitting using Eq. (2). *Red circles* – data from [47] shifted along the vertical axis.

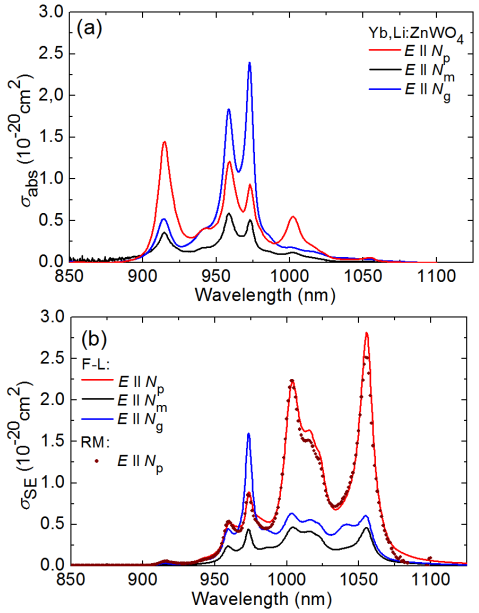

Figure 3. RT spectroscopy of a 1.8 at.% Yb^{3+},Li^{+}:$ZnWO_4$ crystal: (a) absorption cross-section, σ_{abs}, spectra; (b) stimulated-emission cross-section, σ_{SE}, spectra. The light polarizations are $\boldsymbol{E} \parallel N_p, N_m, N_g$. The σ_{SE} values are calculated using the F-L formula, Eq. (3). For light polarization $\boldsymbol{E} \parallel N_p$, the results on σ_{SE} calculated with the reciprocity method (RM), Eq. (4), are given for comparison.

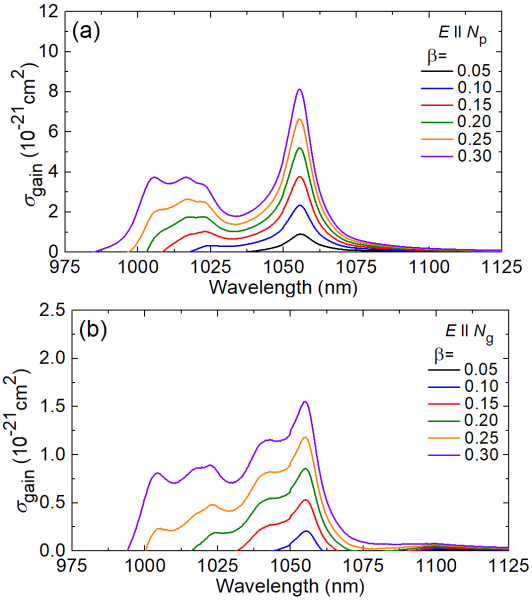

Figure 4. RT gain cross-section, $\sigma_{gain} = \beta\sigma_{SE} - (1 - \beta)\sigma_{abs}$, spectra for the $^2F_{5/2} \leftrightarrow {}^2F_{7/2}$ transition of Yb^{3+}:$ZnWO_4$. The light polarizations are (a) $\boldsymbol{E} \parallel N_p$ and (b) $\boldsymbol{E} \parallel N_g$. $\beta = N_2(^2F_{5/2})/N_{Yb}$ is the inversion ratio, N_2 is the population of the upper laser level ($^2F_{5/2}$).

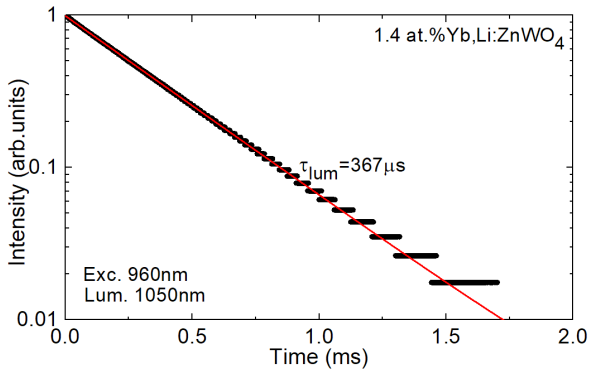

Figure 5. RT luminescence decay curve for thin (t <100 μm) cleaved plates of 1.4 at.% Yb^{3+},Li^{+}:$ZnWO_4$ crystal, λ_{exc} = 960 nm, λ_{lum} = 1050 nm. *Symbols* – experimental data, *line* – single-exponential fit.

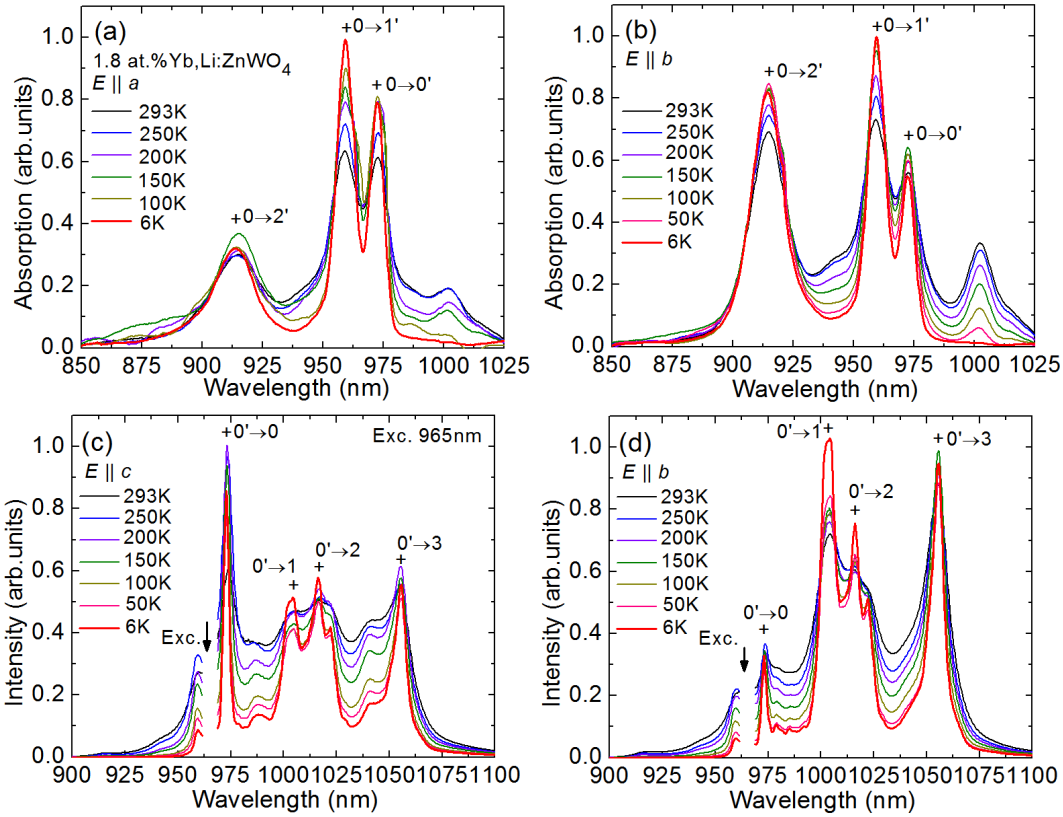

Figure 6. LT (6-293 K) spectroscopy of a 1.8 at.% Yb^{3+},Li^{+}:$ZnWO_4$ crystal: (a,b) absorption spectra for light polarizations (a) ***E*** || ***a*** and (b) ***E*** || ***b***; (c,d) luminescence spectra for light polarizations (c) ***E*** || ***c*** and (d) ***E*** || ***b***, λ_{exc} = 965 nm.

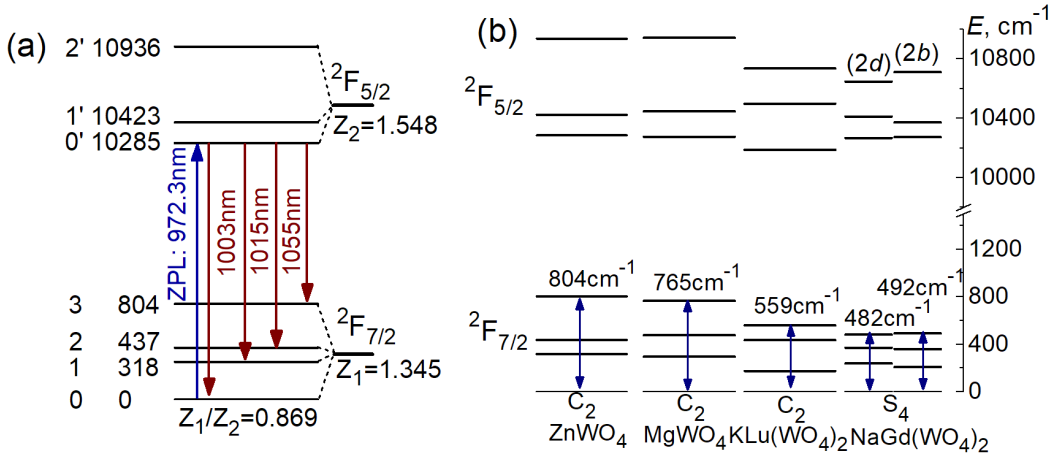

Figure 7. Crystal-field splitting for Yb^{3+} ions in $ZnWO_4$: (a) Scheme of the Stark sub-levels; the *blue arrow* denotes the zero-phonon line (ZPL) transition in absorption, red arrows denote the transitions in emission at 6 K. $Z_1(Z_2)$ are the partition functions for the lower(upper) multiplets; (b) a comparison of the crystal-field splitting for Yb^{3+} ions in $ZnWO_4$, $MgWO_4$ [5], $KLu(WO_4)_2$ [8] and $NaGd(WO_4)_2$ [22] tungstate crystals, C_2 and S_4 – site symmetries.

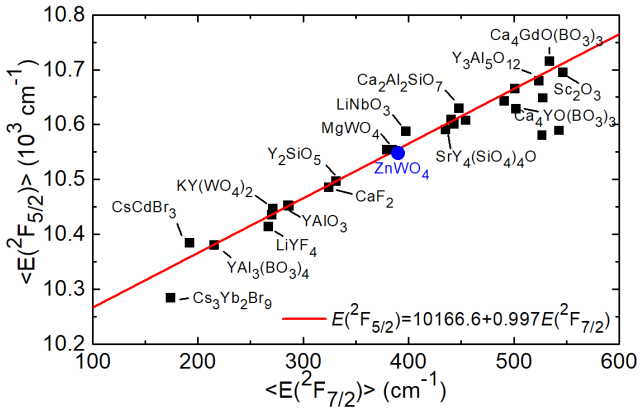

Figure 8. Barycenter plot for Yb^{3+} ions in various crystals. The *blue circle* denotes $ZnWO_4$. The *red line* denotes a linear fit through all the points.

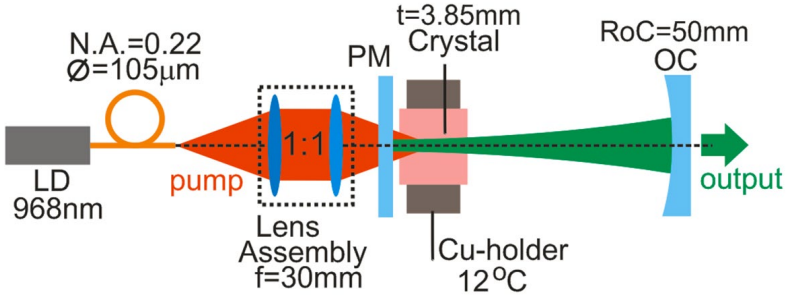

Figure 9. Scheme of the diode-pumped 1.8 at.% Yb^{3+},Li^+:$ZnWO_4$ laser: LD – laser diode, PM – pump mirror, OC – output coupler, RoC – radius of curvature.

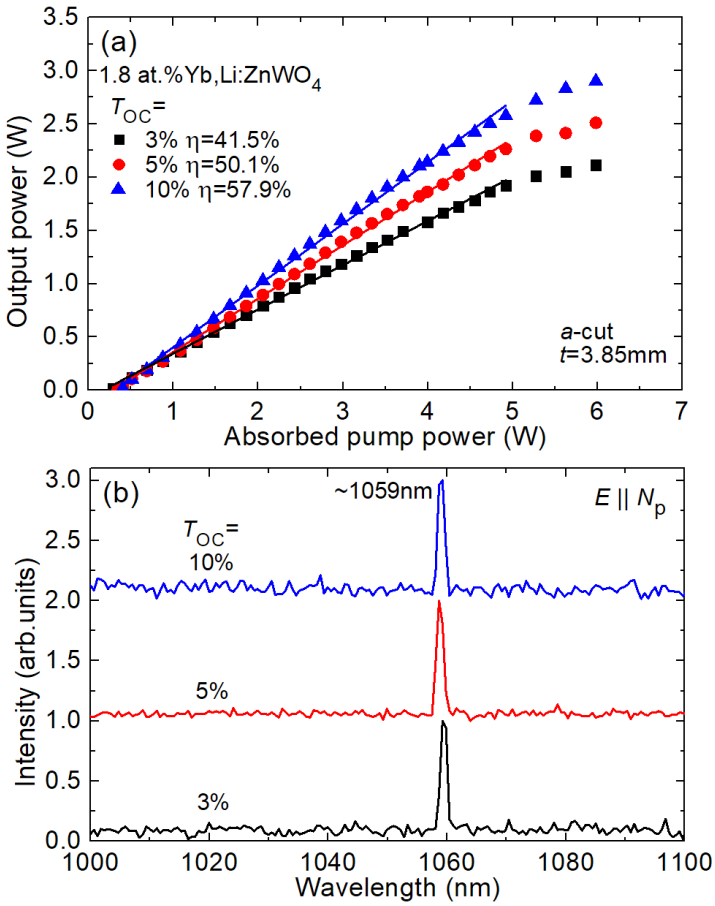

Figure 10. Diode-pumped 1.8 at.% Yb^{3+},Li^{+}:$ZnWO_4$ laser: (a) input-output dependences, η – slope efficiency; (b) typical laser emission spectra. The crystal is ***a***-cut. The laser emission is linearly polarized (***E*** || N_p).